frontiers in Energy Research

ORIGINAL RESEARCH
published: 12 September 2019
doi: 10.3389/fenrg.2019.00100

Rational Selection of Carbon Fiber Properties for High-Performance Textile Electrodes in Bioelectrochemical Systems

*Liesa Pötschke[1], Philipp Huber[2], Sascha Schriever[2], Valentina Rizzotto[3], Thomas Gries[2], Lars M. Blank[1] and Miriam A. Rosenbaum[4,5]**

[1] Institute of Applied Microbiology, Aachen Biology and Biotechnology, RWTH Aachen University, Aachen, Germany, [2] Institut für Textiltechnik, RWTH Aachen University, Aachen, Germany, [3] Institute of Inorganic Chemistry, RWTH Aachen University, Aachen, Germany, [4] Bio Pilot Plant, Leibniz Institute for Natural Product Research and Infection Biology, Hans-Knöll-Institut, Jena, Germany, [5] Faculty of Biological Sciences, Friedrich-Schiller-University, Jena, Germany

Novel applications of bioelectrochemical systems (BES) are emerging constantly, but the majority still lacks economic viability. Especially the use of electrochemical system components without adaptation to BES requirements causes poor exploitation of the potential system performance. The electrode material is one central component that determines BES performance. While commercial carbon fiber (CF) fabrics are commonly used, their customizability as two- or three-dimensional electrode material for BES is rarely investigated. Using pure cultures of *S. oneidensis* MR-1, we identified CF properties impacting bacterial current generation: (1) The removal of the sizing (protective coating) is of great importance for all the fibers studied, as it acts as an electrical insulator. By desizing, the maximum current density (j_{max}) is increased by up to 40-fold. (2) Alteration of the filament surface chemistry results in an accelerated initial development of current generation, but the maximum current density (j_{max}) is hardly affected. (3) A specific yarn structure, the stretch-broken yarn, supports exceptionally high current densities. The good electrode performance is correlated to the presence of free filament ends (responsible for 41% current increase), which are characteristic for this yarn. (4) Moreover, a combination of these free filament ends with a high degree of graphitization enhances electrode performance of a commercial fabric by 100%. The results demonstrate that the CF selection can greatly influence the achievable electrode performance of CF fabrics, and thereby contributes to rational engineering of CF based electrodes that can be tailored for the many BES applications envisaged.

Keywords: carbon fiber electrode, carbon fabric, *S. oneidensis* MR-1, microbial fuel cells, chemical surface activation, desizing, electrical conductivity

OPEN ACCESS

Edited by:
Uwe Schröder, Technische Universitat Braunschweig, Germany

Reviewed by:
Annemiek Ter Heijne, Wageningen University & Research, Netherlands
Benjamin Erable, Centre National de la Recherche Scientifique (CNRS), France

****Correspondence:***
Miriam A. Rosenbaum
miriam.rosenbaum@leibniz-hki.de

Specialty section:
This article was submitted to Bioenergy and Biofuels, a section of the journal Frontiers in Energy Research

Received: *25 June 2019*
Accepted: *30 August 2019*
Published: *12 September 2019*

Citation:
Pötschke L, Huber P, Schriever S, Rizzotto V, Gries T, Blank LM and Rosenbaum MA (2019) Rational Selection of Carbon Fiber Properties for High-Performance Textile Electrodes in Bioelectrochemical Systems. Front. Energy Res. 7:100. doi: 10.3389/fenrg.2019.00100

INTRODUCTION

Bioelectrochemical systems (BES) unlock novel bioeconomic technologies by utilizing the microbial ability of extracellular electron transfer to a solid electrode (Santoro et al., 2017). Remarkably, the transition from lab to full-scale is not yet accomplished for most BES applications. A closer look suggests that recent successful implementations of BES are restricted to special

and niche applications in which the BES has no or few competing technologies or provides an added ecological value (reviewed by Gajda et al., 2018). This can be a combined waste treatment with electricity generation in areas of low infrastructure (Ieropoulos et al., 2016; Walter et al., 2018) or avoiding costly maintenance in the case of benthic fuel cells powering remote sensors (Tender et al., 2008; Donovan et al., 2013; Ewing et al., 2017). In such cases, a full exploitation of the microbial potential is not necessary and low-cost standard commercial materials (carbon felts, ceramic separators) perform satisfactorily. In contrast, large scale wastewater/remediation applications (Hiegemann et al., 2016; Lu et al., 2017b; Wang et al., 2017) or high-tech applications such as the production of specialty chemicals (Raes et al., 2016; Streeck et al., 2018) are not yet ready for marketing, because here, high efficiencies are mandatory for economic operation and competitiveness with established technologies.

Considerable effort has been put into the engineering of BES toward various enhanced performance parameters, which have been extensively reviewed elsewhere (Janicek et al., 2014; Santoro et al., 2017). Especially, the core element bioanode is in the focus of research and development. Independent from the electrode material, chemical and physical modifications have been applied successfully to increase electrode performances in BES (He et al., 2011; Guo et al., 2013; Kipf et al., 2013; Artyushkova et al., 2015; Baudler et al., 2015; Champigneux et al., 2018; Pierra et al., 2018; Moß et al., 2019).

In our preliminary work, we identified carbon fiber (CF) based textile electrodes as all-rounder electrode material, since they combine all preferred features for large scale applications, i.e., large specific surface area in the (m^2/g) range, good mechanical and chemical stability, customizable flexibility and porosity at µm up to cm scale; all of which enable high electrode packing densities (Morgan, 2005). Own previous pure culture screening showed a broad range of bioelectrochemical activity for different commercial carbon fiber materials (**Figure S1**). Although CF fabrics are widely used in lab-scale BES studies, they are usually not favored for large-scale BES, because they are considered too costly in manufacturing (Wang et al., 2009; Santoro et al., 2017). However, authors rarely acknowledge the extremely wide variety within the types of textile materials and especially the CF. Usually, the exact properties of the used materials are not reported, comparing e.g., just "carbon cloth" or "carbon mesh" without mentioning the underlying fiber (Wang et al., 2009; Blanchet et al., 2016). In contrast, the numerous high-tech applications of CF in fiber reinforced plastics, such as light-weight construction in aerospace, automobile, or reinforcement of sports and medical equipment, have created a worldwide industry with well-established processing technologies and customizable products.

CF are derived from organic precursors with preferably high carbon yield (i.e., low amount of non-C atoms that will vanish during carbonization). The most common precursors are polyacrylonitrile (PAN) and pitch with a market share of 96 and 3%, respectively (Das et al., 2016), and a substantial difference in application and especially price (typically around 20 €/kg for PAN and around 100 €/kg for pitch based CF). Pitch CF generally exhibit lower specific electrical resistivities than PAN CF, but the ranges are not far from overlapping (ρ_{fiber} = 0.3–0.8 vs. 1–2 mΩ·cm, own preliminary market screening, data not shown). The focus of this study was on PAN CF due to their advantages regarding price and availability.

The simplified standard production processes for PAN CF woven fabrics are depicted in **Figure 1**. Under tensile stress, the fibers are stabilized in air at 200–300°C (cyclization and increasing density of the polymer = oxidized PAN, PANOX), and subsequently carbonized by means of high temperature (1,000–1,700°C) in an inert atmosphere. The resulting CF are bundles of thousands of parallel filaments with diameters of 5–7 µm (Morgan, 2005). This structure provides the large specific surface area [m^2/g], which makes CF fabrics such popular electrode materials. The most common fiber type is the continuous multifilament roving (CM), which contains parallel, endless filaments with little to no twist. CM are also referred to as tows and classified by their tow size (xK = x,000 filaments). A CM may be converted into the less common stretch-broken yarn (SB). The result is a twisted bundle of filaments with an approximately length in the order of magnitude of 10 cm. The stretch-breaking process can be either applied to the carbonized CM or to the stabilized fiber, which is then carbonized at fabric level. Here, we consider only the latter type of SB fabrics (production route 2, **Figure 1**), which are usually referred to as PANOX fabrics.

The electrical properties of a carbon filament are determined by the purity and orientation of their basal planes, i.e., carbon grids along which electrons are conducted. The planes are stacked onto each other and electrons flow best in-plane, i.e., in-filament direction (Dutta, 1953; Windhorst and Blount, 1997). During carbonization, tensile stress and process temperature regulate CF electrical properties. CF carbonized at 1,000–1,700°C contain 92–98% atomic carbon (at.%). Higher temperatures above 2,000°C achieve graphitized fibers with a carbon content over 99 at.% (Morgan, 2005). After carbonization (graphitization), CF are stiff and brittle. Unlike SB, which are carbonized as a whole fabric, CM need to be subjected to a finishing step prior to textile processing. This includes a chemical surface activation and the subsequent application of a protective coating (sizing). Surface activation enhances the adhesion of the sizing via introduction of foreign atoms and residues into the carbon grid (Kozlowski and Sherwood, 1986; Alexander and Jones, 1996; Severini et al., 2002). The sizing itself is based on polymers like epoxy resins, polyurethanes, and others, which are able to reduce friction and wear on the fibers during the textile processing and enable the fiber-matrix adhesion in the production of CF reinforced plastics. On the other hand, the sizing usually acts as an electrical insulator, which is why this coating needs to be removed before CM can be employed as BES electrode material. Finally, a second round of chemical surface activation may be applied in order to enhance the fiber-bacteria interaction of the CF electrode (the first surface activation is usually not sufficiently stable, see Jones and Sammann, 1989). The introduction of polar and charged functional groups will mainly increase the initially poor

Abbreviations: BES, bioelectrochemical system; CE, coulombic efficiency; CF, carbon fiber; CM, continuous multifilament roving; MFC, microbial fuel cell; PAN, polyacrylonitrile; SB, stretch-broken yarn; TGA, thermogravimetric analysis; XPS, X-ray photoelectron spectroscopy.

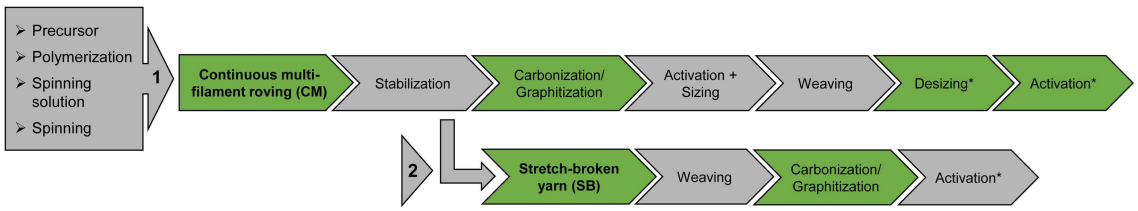

FIGURE 1 | Simplified general production process of woven CF fabrics (PAN based) made from either continuous multifilament rovings (1) or stretch-broken yarns (2). Stars mark the steps that are added especially for the application in BES. The parameters investigated in this study are highlighted in green (fiber type, degree of graphitization, desizing, and 2nd chemical surface activation).

TABLE 1 | Properties of commercial PAN CF used in this study.

Abbreviation	Feature of interest	Manufacturer	Product name	Tow size
HTS40	Good performance in previous BES fiber screening	TT	Tenax® E HTS40-F13	12K
CT50	Equivalent product to HTS40, but different processing	SGL	C T50-4.0/240-E100	50K
T300	Standard fiber and sizing	TO	Torayca® T300-40B	3K

SGL, SGL Carbon, Germany; TO, Toray Industries, Inc., Japan; TT, Teijin Carbon Europe GmbH (previously Toho Tenax), Japan/Germany.

wettability of the fiber surface (Qian et al., 2010), thus enhancing its accessibility.

With this study, we aimed at laying the foundation for a comprehensive customized engineering of CF woven electrodes for BES. With respect to the production process chain, we investigated possibly relevant parameters, such as yarn macrostructure (CM or SB), the filament conductivity, desizing, and 2nd surface activation, and evaluated their influence on electrode performance. To minimize biological variability during this comparative evaluation of material properties, we utilized the robust anodic electroactivity of *S. oneidensis* MR-1 for this work. One step beyond these crucial fiber and fabric materials properties, also the 3D fabric architecture will be an important parameter for successful CF electrode utilization in diverse BES applications. However, since this would overload the scope of the presented work, it will be followed up in subsequent publications.

MATERIALS AND METHODS

All textile products were denominated following international terminology standards (ASTM D123).

Preparation and Physical Characterization of Carbon Fiber and Fabric Samples

Fibers were subjected to a preparative physical characterization prior to evaluation as BES electrodes. The workflow was electrical resistivity measurement (**Table S1**), tribological characterization and/or artificial introduction of filament breaks (Tribology Test Rig), desizing (Desizing), and chemical surface activation (Chemical Surface Activation of Carbon Fibers), if applicable. Fabrics were desized (Desizing), and physical characteristics were obtained from manufacturer's datasheets. All materials were based on PAN precursor. An overview of the relevant properties of all included CF is given in **Table 1**, extended technical properties of these fibers are given in **Table S1**. **Table 2** introduces commercial and modified fabrics used in this study, extended technical properties can be found in **Table S2**. SIGRATEX® fabrics were especially selected for chapter Effect of Filament Conductivity and Fiber Type on Bacterial Current Generation, since both their carbonized and graphitized equivalents are commercially available. For the SB fabrics, technical details about fibers cannot be provided, since the carbonization process occurs on fabric level (**Figure 1**). High tenacity CM (like CT50 and HTS40, **Table 1**) were used for the production of SIGRATEX® CM fabrics.

The electrical resistivities of CF fabrics are in the same order of magnitude as the respective single CF. However, reliable standardized measurement methods do not exist on fabric level and the measurement errors tend to be high, which is why specific fabric resistivities are not given in **Table 2**.

Tribology Test Rig

For the introduction of intended breaks (damaged multifilament rovings, results Effect of Fiber Type on Bacterial Current Generation), a customized indenter with sharpened grooves was fabricated in-house. Fiber strengths were assessed according to ASTM D3108 (registered method to characterize to what extent fibers are prone to filament breakage) using an in-house test rig with the following operational parameters: looping angle 180°; 5 m/min yarn throughput, test interval 5 min (tested fiber length 25 m), initial load of filament break sensors before/after indenter 5 N/12 N. The resulting fiber damage is expressed as statistical average amount of broken filaments in a random cross-section of the roving [% of x K filaments]. Fibers with filament damage exceeding 10% could not be processed further since they disassembled in the non-twisted configuration. The obtained

TABLE 2 | CF fabrics used in this study.

Abbrevation	Feature of interest	Manufacturer	Product name	Fiber type
SB_{low}	Low C-content	SGL	SIGRATEX® C W270-TW2/2/CA	SB
$SB_{moderate}$	Moderate C-content	SGL	SIGRATEX® C W230-TW2/2/GR	SB
SB_{high}	High C-content	SGL	SIGRATEX® C W230-TW2/2/GR (graphitized at 2,800°C)	SB
CM_{low}	Low C-content	SGL	SIGRATEX® C W245-TW2/2	CM, 3K
$CM_{moderate}$	Moderate C-content	SGL	SIGRATEX® C W230-TW2/2/GR	CM, 3K
CM_{high}	High C-content	SGL	SIGRATEX® C W230-TW2/2/GR (graphitized at 2,800°C)	CM, 3K
T300 fabric[a]	Not surface activated during production, standard fiber and sizing	CT	CT200L-200	CM, 3K

SGL, SGL Carbon, Germany; CT, CARBO-TEX, Germany; SB, stretch-broken yarn; CM, multifilament roving. Except for SB (do not contain sizing), all fabrics were pyrolytically desized (N_2 atmosphere). SB_{high} and CM_{high} are not commercially available and were obtained from $SB_{moderate}$ and $CM_{moderate}$ by further graphitization in a muffle furnace under argon atmosphere at 2,800°C, 30 min holding time.

[a] The T300 standard fabric was fabricated from fiber Torayca® T300-40B and was mainly used to develop and evaluate a suitable desizing methodology.

range of fiber damage was 2.4–7.2%. Damaged fibers are referred to as "Dx" hereafter.

Desizing

In parallel to the screening of commercial CF for suitable material properties, a desizing method was established to be applicable to all CF based electrodes. Tested desizing methods were industrial washing agents (used according to manufacturer's protocols), Soxhlet extraction (removal of sizing by organic solvents) with acetone/20 cycles, as well as pyrolysis (burning off the sizing). Pyrolysis was identified as final method of choice and subsequently applied for all CF electrodes presented here. An inert process gas was chosen, since desizing under air may alter the CF surface (Morgan, 2005). This can lead to either negative effects when the fiber conductivity is affected, or positive effects when the surface chemistry is modified to be more hydrophilic. All fabrics were desized in a muffle furnace under N_2 atmosphere at 500°C, 20 min holding time. For single fibers, a continuous operation tube furnace (N_2 atmosphere) was used, which required differing operational parameters: 700°C with a retention time of 2–4 min depending on the fiber thickness. Quantitative control of desizing quality was performed via thermogravimetric analysis (TGA) in a TGA/DSC 1, Mettler Toledo, Germany. Samples were heated under N_2 atmosphere to 550°C within 110 min and the resulting weight loss was recorded. Qualitative control of desizing was performed via SEM (LEO 1450VP, Zeiss, Germany) with 15 kV accelerating voltage.

Chemical Surface Activation of Carbon Fibers

The two CM used for surface activation experiments were C T50-4.0/240-E100 (hereafter CT50) and Tenax® E HTS40-F13 (hereafter HTS40) from two different manufacturers. The material specifications of both fibers were comparable (**Table S1**), only the filament numbers resulted in different electrode fiber lengths (27 and 114 mm for CT50 and HTS40) to achieve a fixed filament surface area (300 cm^2) as a standardization parameter. The resulting electrical resistances of the fiber electrodes were 1.2 and 1.3 Ω for CT50 and HTS40, respectively. Desized fibers were activated by electrolysis or plasma treatment, both methods having industrial relevance regarding ease of process chain integration and scale-up. Operational parameters for electrolysis were 18% NH_3HCO_3, fiber connected to an external power supply as anode, graphite plate as counter electrode, applying 3 A/24 V for 240 s at 22°C. Plasma treatments were kindly conducted by Diener electronic GmbH & Co. KG, Germany; parameters were $3{\cdot}10^{-4}$ bar, continuous gas flow 30 sccm, 15 min using either oxygen, ammonia, or ambient air as process gas.

HTS40 fibers had shown a good performance in previous electrode screenings (single fiber BES, not shown). Therefore, they were selected as model fibers and were further characterized by contact angle and X-ray photoelectron spectroscopy (XPS) analysis. The contact angle measurement was conducted with a K100 SF (Krüss GmbH, Germany), which is designed for single carbon fibers (the fiber is pulled out from a wetting liquid and the contact angle is calculated from the resulting force). XPS survey spectra were recorded at a pass energy of 60 eV using a Phoibos 100 analyzer with a CCD detector (SPECS Surface Nano Analysis GmbH, Germany). High-resolution spectra of the C 1s, O 1s, and N 1s peaks were recorded at a pass energy of 20 eV.

General BES Setup and Analyses

For the preculture, *Shewanella oneidensis* MR-1 (ATCC® 700550™) was cultivated overnight in LB medium (LB Lennox, Carl Roth, Germany) at 30°C. For the bioelectrochemical experiments, the modified M4 medium (pH 6.8, solution conductivity 19 mS/cm) contained per liter: K_2HPO_4 2.21 g; KH_2PO_4 0.99 g; $NaHCO_3$ 0.168 g; $(NH_4)SO_4$ 1.189 g; NaCl 7.305 g; HEPES buffer 1.192 g; yeast extract 0.5 g; tryptone 0.5 g; $CaCl_2 \cdot H_2O$ 0.071305 g; 100x mineral mix stock as in Beg et al. (2012) 10 ml. 18 mM sodium D/L-lactate (60%$_{w/w}$ syrup, Sigma Aldrich, Germany) was used as carbon source and was added after autoclavation. Experiments were conducted at room temperature (recorded fluctuation 23.5–26°C). All potentials were controlled (potentiostats: VMP-3,

BioLogic Science Instruments, France; Ivium-n-Stat, Ivium Technologies, Netherlands; in-house designed handheld potentiostats controlled via the software tool Labview, Texas Instruments, TX, USA) at + 0.2 V against a $Ag/AgCl_{sat.KCl}$ reference electrode that was freshly prepared in-house prior to each experiment. Maximum electrical current density j_{max} was determined from one complete batch in single fiber BES. For fabric BES, up to 3 batches were run until the current generation did not increase any further, and j_{max} was determined considering all batches.

The optical density at 600 nm (OD_{600}), pH and concentrations of lactate and acetate (HPLC on Metab-AAC column, 300 × 7.8 mm, Isera GmbH, Germany; in 5 mM H_2SO_4 mobile phase, 0.6 ml/min, 30°C) were tracked for the whole experimental duration. Furthermore, selected bioelectrode samples were cut out and analyzed by scanning electron microscopy (SEM) with 10 kV accelerating voltage on a Zeiss DSM 982 Gemini microscope (Zeiss, Germany). The sample preparation procedure included fixation in 2.5% glutaraldehyde, storage in ethanol, and drying by hexamethyldisilazane, and sputtering with a 20 nm gold layer. Where reported, riboflavin concentrations of filtered (0.2 µm pore size) samples were analyzed spectrophotometrically in reference to a riboflavin standard (Carl Roth GmbH & Co. KG, Germany), excitation/emission 450/530 nm as reported in Lu et al. (2017a). Coulombic efficiencies (CEs) were calculated based on the incomplete lactate oxidation to acetate, yielding 4 electrons per molecule of consumed lactate, which *S. oneidensis* MR-1 performs stoichiometrically under anoxic conditions (Pinchuk et al., 2011).

Single Fiber BES

Single carbon rovings were configured in a loop-like structure and attached to graphite rods (grade EDM-3 (specific electrical resistivity 1.56 mΩ·cm), Ø 30 mm, Novotec, Germany) using conductive carbon cement (Leit-C, Sciences Services GmbH, Germany). Common adhesive tape delimited the desired immersed fiber length that performed as working electrode. The fiber length was normalized to a theoretical BET surface area of ∼300 cm^2 (calculated by considering single filaments as perfect solid cylinders), assuming that the available electrode surface area is the most crucial parameter for bacterial interaction (Chen et al., 2011; He et al., 2011). A longer graphite rod (grade EDM-3, Ø 30 mm, Novotec, Germany, immersed length 50 mm) was used as counter electrode. The reactors consisted of laboratory glass bottles of 100 ml working volume. Instead of a lid, a 3 mm thick butyl rubber served as septum for sampling and held the electrodes in place. PTFE tape was applied at the electrode-rubber contact points for additional sealing. The complete reactors were sterilized by standard wet autoclavation (1 bar, 121°C for min. 20 min) with exception for surface activated fibers, which were sterilized separately from the reactor by applying 70% ethanol (including the untreated controls). All reactors were filled with N_2-degassed medium in an anaerobic chamber to minimize the initial oxygen content in the system. These single fiber BES were run in triplicates or duplicates.

In deviation to the standard setup, fragile fibers of the filament break experiments (chapter Effect of Fiber Type on Bacterial Current Generation) were configured straight and stabilized by tooth picks as shown in **Figure 4**. In this case, the total fiber length of 12 cm (317 cm^2 filament surface) was split into two to fit in the reactor. The counter electrode was wrapped in a separator (0.2 µm Supor®-200 PES filter membrane, Pall Corporation, NY, USA) to prevent short-circuits between electrodes. T0 describes non-twisted fiber electrodes, while Tx fibers contain 12 twists of 180°. This way, T0 yielded an open electrode structure with freely floating single filaments, while Tx yielded a tight packing of the filaments and displayed a structure that was comparable to a commercial twisted yarn (**Figure 4**). The working volume was increased to 200 ml to fit the straight electrode and stirred at 100 rpm (50 mm magnetic stir bar) to enhance chemical species transport through the separator. An exemplary setup is shown in **Figure S2B**. The CEs of single fiber experiments were lower than in the plate reactors (chapter Fabric BES), around 26 ± 13% (n = 27) for the original setup and 7 ± 2% (n = 24) in the modified setup for broken fibers. The reduced CE was due to the lower electrode packing density—especially in the modified setup—and consequently electron loss to oxygen that slowly intruded into the headspace (**Figure S2A**). However, this oxygen was scavenged by a biofilm formed at the liquid-headspace interface (**Figure S2C**). This way, the single fiber setup still yielded filament current densities of one magnitude higher than comparable setups (∼1 vs. 0.13 $\mu A/cm^2_{filament}$ at the same poised potential in Lu et al., 2017a) and was appropriate for the investigation of fiber material properties independently from fabric level parameters such as weave density. However, overall biomass or mediator production could not be meaningfully connected with bacterial current generation. The modified single fiber BES were run in 6 biological replicates to compensate for possible influences by the low packing density.

Fabric BES

The working electrodes were constructed from 45 × 120 mm carbon fiber fabrics that were attached to graphite clamps. A graphite rod (grade EDM-3, Ø 30 mm, Novotec, Germany, immersed length 145 mm) was used as counter electrode. The flat-plate-type reactor consisted of two rectangular PEEK frames (10 × 148 × 55 mm) with glass walls that were pressed together along with a synthetic rubber gasket (EPDM Ø 6 mm, Hug Industrietechnik, Germany). Each of the frames held working/counter electrode and the reference electrode (**Figure S3**). A total working volume of 400 ml was recirculated at 20 ml/min between the reactor (net liquid volume 120 ml) and an external stirred recirculation bottle which allowed for mixing and continuous nitrogen sparging (∼0.5 L/min) of the electrolyte. All tubings were of low gas permeability and appropriate wall thickness (connection tubes: Norprene® A-60-G and pump tubes: Tygon® F-40-40-A, both ProLiquid GmbH, Germany; inner diameter 1.6/0.51 mm; wall thickness 1.6/0.9 mm; permeability for O_2 is 200/22 $cm^3/([cm\ Hg]\cdot 10^{-10})$ at 25°C, respectively]. CEs ranged around 43 ± 23% (n = 19), which are high for *S. oneidensis* based BES (literature values range from 10 to 40%; Watson and Logan, 2009; Rosenbaum et al., 2011; Kipf et al., 2013; Engel et al., 2019). Fabric BES were run in biological triplicates or duplicates.

TABLE 3 | Degrees of desizing after application of varying desizing methods for woven fabrics made from CF T300 (initial sizing amount 0.992%$_{w/w}$).

Desizing method	Process medium	Degree of desizing [%]
None	–	0
Pyrolysis	N_2	83.3
Soxhlet extraction	Acetone	73.8
	Ethanol	51.4
	Petroleum ether	16.0
Washing agents	Rucogen DFL-200 (Rudolf Group, Germany)	62.7
	Sulfaton D (Bozzetto GmbH, Germany)	57.5
	Tanaterge® Advance (Tanatex Chemicals, Netherlands)	70.7
	Propetal140/Sulfetal 4105 (mix) (Zschimmer & Schwarz, Germany)	44.8

Parameters were: Pyrolysis 500°C, 20 min; Soxhlet extraction 20 cycles; washing agents according to manufacturer's protocol. Degree of desizing expresses weight loss of a desized CF compared to the weight loss of the non-desized control as determined by TGA.

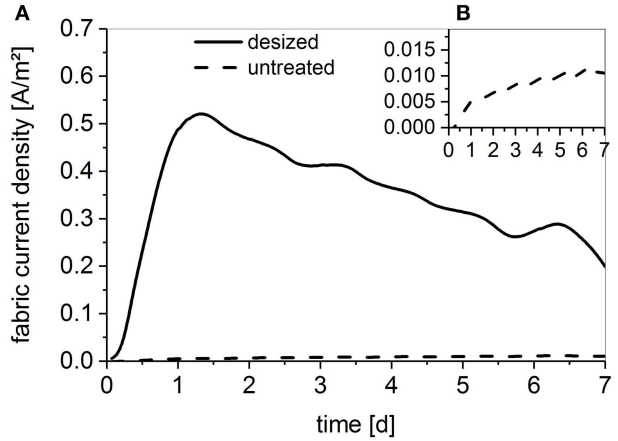

FIGURE 2 | (A) Bacterial current generation on T300 plain woven fabrics (average from $n = 2$); straight lines, pyrolytically desized (N_2 atmosphere); dashed lines, untreated (with intact sizing). Insert **(B)** shows untreated fabrics with smaller y-axis scale.

TABLE 4 | Physical characterization of surface activated HTS40 fibers.

Treatment	Contact angle [°]	O [at.%]	N [at.%]	C [at.%]
Not activated	76.53	5.46	1.81	92.73
NH_3 plasma	42.46	5.88	5.92	88.21
Electrolysis	15.68	15.27	6.64	78.09
Air plasma	9.26	12.63	3.06	84.31
O_2 plasma	8.52	18.11	1.77	80.13

All fibers were desized prior to surface activation. Contact angles were measured on a Krüss K100 SF (Wilhelmy method), atom contents via XPS. Other foreign atoms than O and N were not analyzed.

RESULTS

Establishing a Reliable Desizing Method for CF Electrodes

Standard T300 fabrics (**Table 2**) were used to establish a suitable desizing method for CF fabrics at the beginning of the project. The underlying fibers Torayca® T300-40B (**Table 1**) contain a common sizing type, i.e., epoxy resin or similar, but the exact compositions are company secrets (datasheet: "epoxy and phenolic compatible"). The amounts of sizing as analyzed by TGA were 0.992%$_{w/w}$ (percent weight of total CF + sizing weight), which matches the manufacturer's specifications (1%). The tested methods were pyrolysis under inert atmosphere, industrial washing agents, and Soxhlet extraction. All desizing methods were compared by means of their achieved degree of desizing (%), i.e., the weight loss of a desized CF compared to the weight loss of the non-desized control as determined by TGA (**Table 3**).

Desizing by pyrolysis achieved the highest degree of desizing. Regarding the electrode performance in BES, the pyrolytic removal of the sizing accounted to an ∼45-fold increase of j_{max} for a desized T300 fabric (**Figure 2**). The result was confirmed on single fiber level (∼10-fold increase of j_{max} by desizing, $n = 1$, not shown). One other method, Soxhlet extraction with acetone, achieved similarly high degrees of desizing as N_2 pyrolysis and was able to compete with the respective performance gain in the BES (not shown). However, Soxhlet extraction produces solvent waste and is more complicated for industrial scale-up. The washing agents were clearly inferior to pyrolysis and Soxhlet extraction, since the desized electrodes performed unsatisfactorily in the BES (not shown). The degrees of desizing were mainly consistent for another fiber type with epoxy-compatible resin (**Tables S1**, **S3**). We consequently applied N_2 pyrolysis as the desizing method of choice for all other CF (fabrics) in this work. Process parameters (e.g., retention time) were adapted, where necessary, in order to ensure a complete sizing removal.

Effect of Chemical Surface Activation of CF on Bacterial Current Generation

The two equivalent commercial PAN-based carbon fibers CT50 and HTS40 (**Table 1** and **Table S1**) were used for surface activation experiments. HTS40 fibers served as model fibers, which were additionally subjected to surface characterization by contact angle and XPS measurements.

Physical and Chemical Characterization of Surface Activated CF

All surface activation methods achieved a decrease in contact angle, i.e., increase in wettability, and introduced foreign atoms into the HTS40 fiber surface (**Table 4**).

Oxygen containing functional groups were introduced into the carbon surface by all methods. In NH_3 plasma treated samples, this amount was small and is unlikely related to the high-purity process gas. It was rather related to previously adsorbed atmospheric O_2, which appeared mainly as C-O bonds

TABLE 5 | High-resolution XPS spectra analysis of surface activated HTS40 fibers.

	C 1s				N 1s			O 1s		
Treatment	**C-C**	**C-O**	**O-C=O**	**C=O**	**N-C**	**N-?**	**N-O**	**O=C**	**O-C**	**O-N**
Not activated	75.73	13.14	–	3.86	1.4	0.41	–	2.83	2.83	–
NH_3 plasma	66.77	15.95	–	5.49	5.92	–	–	0.69	4.51	0.68
Electrolysis	57.45	12.61	–	8.03	5.74	–	0.9	4.97	10.3	–
Air plasma	60.22	13.55	4.03	6.51	2.64	0.42	–	10.35	2.28	–
O_2 plasma	52.62	13.05	7.04	7.42	1.77	–	–	7.41	10.7	–

Values are given in [%] of the C 1s, N 1s, and O 1s peaks, respectively. N-? refers to other atoms than C and O, which have not been analyzed in more detail.

(hydroxyl groups, since no O-C=O was observed) and, in small portions, in N-O bonds (e.g., imine-N-oxide) in the high-resolution spectra (**Table 5**). All other treatment methods preferably introduced O in the form of C=O or O-C=O (carboxyl/carbonyl groups). Nitrogen containing groups were introduced in lower quantities than oxygen containing groups. This was achieved by all treatments but the O_2 plasma treatment, which even removed a small portion of N from the original fiber surface. Both NH_3 plasma and electrolysis were similarly effective at introducing N as N-C (e.g., amine, imine, pyridone) and in small portions also N-O bonds (e.g., imine-N-oxide).

Characterization of Surface Activated CF in Single Fiber BES

Figure 3 shows the summarized results from single fiber BES (unstirred 100 mL setup, combined filament surface fixed at 300 cm^2). The total number of biological replicates was $n = 3$ for all treatments, except for electrolysis with $n = 2$. Besides j_{max}, the startup current density j_{12h} is given, which assesses effects on the initial bacteria-electrode interaction. The latter is expressed as current density after 12 h, since the initial current increase for the used BES varied in its characteristics, e.g., linear or exponential increase, and the calculation of a specific rate was not possible. A high standard deviation was observed for the activated fiber electrodes. This variation might be connected to the presumable short-term stability of introduced foreign atoms and residues in the carbon filament surface. Although empirical values are not collected in industry due to limited necessity (fibers are sized immediately after surface activation), chemical alterations of the introduced residues is expected by professionals within in the range of several hours to days (Jones and Sammann, 1989). This time frame is short compared to the preparation of the BES setup which takes at least 1.5 days from fiber activation until the start of the experiment. As a consequence, the variances of the samples are probably unequal; and the Welch corrected *t*-test was therefore chosen for statistical significance analysis (significance level < 0.05).

Untreated CT50 and HTS40 achieved similar j_{max} (**Figures 3C,D**), which is in correspondence with their equivalent electrode surfaces and material properties (**Table 1** and **Table S1**), but j_{12h} was higher with HTS40. For HTS40 (**Figures 3B,D**), neither j_{12h} nor j_{max} were significantly altered by any of the activation methods, although air plasma and electrolysis showed some promising trend regarding j_{max} and j_{12h}, which might have been just masked by the high variance of the replicate values.

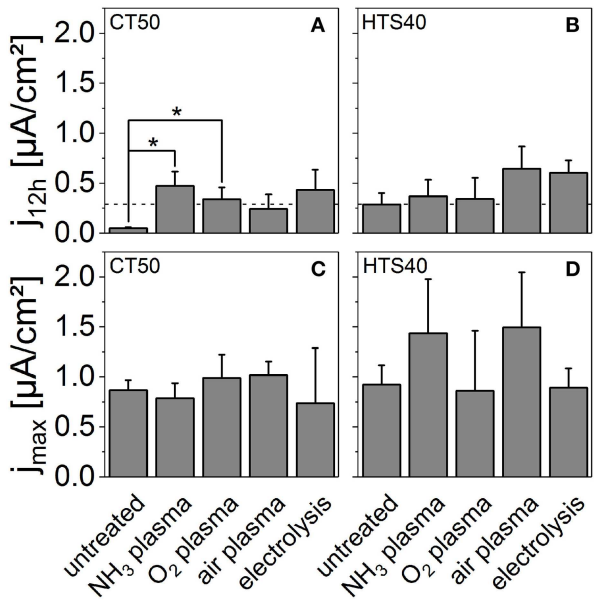

FIGURE 3 | Performances of single carbon fiber electrodes CT50 **(A,C)** and HTS40 **(B,D)**; influence of different surface activation methods on startup current density **(A,B)** and maximum current density **(C,D)**, both normalized to filament surface area (300 cm^2). Non-activated controls are only desized. The j_{12h} level of the untreated HTS40 control is indicated by the dashed horizontal line. Asterisks mark significance levels with $p < 0.05$ (Welch corrected two-sampled *t*-test).

For CT50 (**Figures 3A,C**), j_{12h} was significantly enhanced after surface activation for NH_3 and O_2 plasma ($p < 0.05$) and reached the level of the untreated HTS40. Also for the other two methods all single values were higher than those of untreated fibers, but *P*-values were above 0.05. However, we considered all activation methods capable of enhancing j_{12h} in CT50. Due to the high variance within replicates, quantitative comparisons between the methods were not possible.

Elucidating the High Performance of Stretch-Broken Yarn Based Electrodes

The two features that distinguish the less common SB from the classic CM are free filament ends (**Figure S4**) and a yarn twist.

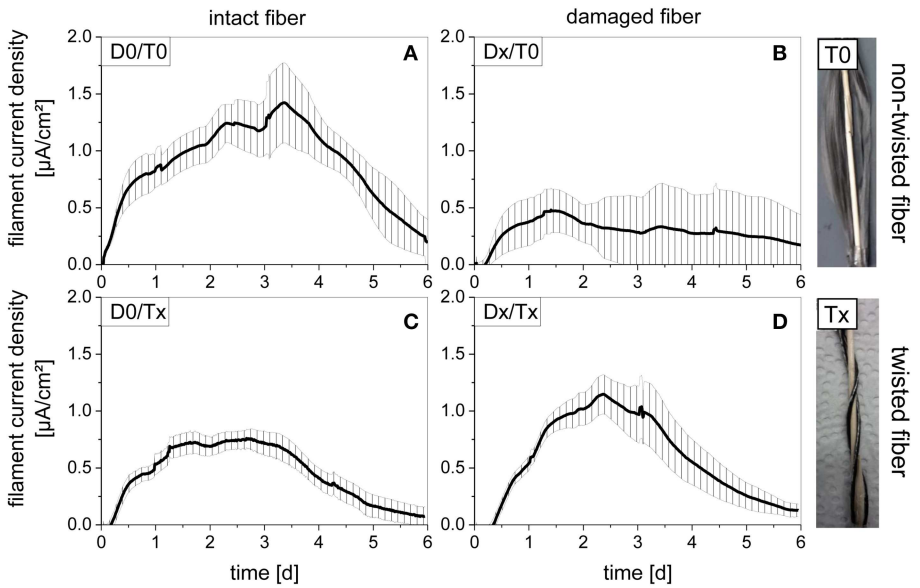

FIGURE 4 | Current density normalized to combined filament surface in single fiber BES (HTS40 CM); **(A,C)** intact fibers and **(B,D)** fibers with introduced breaks. Legend: D0, intact; Dx, damaged; T0, non-twisted **(A,B)**; Tx, twisted yarn **(C,D)**. One electrode consists of two 6 cm fiber pieces. Shown are average values and standard deviations from 6 replicates. Photographs (taken by F. Schmitz) show a representative fiber electrode for non-twisted yarns T0, i.e., open display of filaments, and twisted yarns Tx, which resemble commercial twisted yarns.

SB fabrics had yielded outstanding current densities and material utilization efficiencies in a previous screening (**Figure S1**). We aimed at systematically investigating the influence of the fiber macrostructure (SB vs. CM) on the performance of CF based electrodes in BES.

Effect of Fiber Type on Bacterial Current Generation

Free filament ends and yarn twist were introduced into HTS40 fibers (12K CM) at lab scale in order to reconstruct the industrial production of stretch-broken yarns from multifilaments. Identical CM without tribological treatment served as intact control electrodes. **Figure 4** shows the resulting current generation for all four D/T combinations (D0, intact; Dx, damaged; T0, non-twisted; Tx, twisted CM). In the open fiber structure of T0, the introduced filament breaks reduced current production by 58% (average). In tightly twisted fibers Tx, filament breaks enhanced j_{max} by an average of 41% compared to the intact (twisted) control (Dx/Tx vs. D0/Tx). The twist also resulted in a substantially increased j_{max} (by 93%) and decreased standard deviation compared to the untwisted damaged fibers Dx/Tx vs. Dx/T0. In the intact control, however, the introduction of a twist led to a reduced j_{max} by ∼43% (D0/Tx vs. D0/T0).

For a deeper understanding of the link between free filament ends and bacterial current generation, confocal scanning laser microscopy (CSLM) imaging of different fiber electrodes was performed (see **Supplementary Information**). However, it turned out challenging to find free filament ends in the bulk multifilament and only few were analyzed. The biofilm formation seemed uniform over the filament surface including free ends (**Figure S5**). The single fiber BES setup was not optimized for investigations of the mediated electron transfer due to side reactions with headspace oxygen (**Figure S2A**) and we rather went on to elucidate these mechanisms on fabric level.

Effect of Filament Conductivity and Fiber Type on Bacterial Current Generation

A set of related commercial fabric types was selected in order to verify the role of free filament ends in stretch-broken yarns and elucidate the mechanisms behind their good performance. Besides the filament macrostructure, we selected fabrics with different carbon atom content C [at.%] to vary filament conductivity, which was not possible to study at fiber level because of mechanical instability of graphitized fibers. The model electrodes were commercial SIGRATEX® fabrics made from CM or SB along with their equivalent graphitized products (**Table 2** and **Table S2**, all SGL Carbon, Germany). The samples will be referenced to as SB_{low} and $SB_{moderate}$ (SB = stretch-broken) and CM_{low} and $CM_{moderate}$ (CM = continuous multifilament); with the subscripts expressing the difference in carbon content. Additionally, both $SB_{moderate}$ and $CM_{moderate}$ fabrics were subjected to further graphitization at a higher temperature of 2,800°C, since highly graphitized versions of these fabric were not commercially available. These fabrics were referred to as SB_{high} and CM_{high}. Consequently, we obtained samples with ∼92, > 99, and > 99.9 C at.%. Note that CM and SB fabrics cannot be directly compared, since they differ in their material characteristics (precursor fiber, manufacturing process, filament diameter, and fabric areal weight). **Figure 5** summarizes the results for maximum OD_{600}, maximum current density j_{max} and start-up current density j_{12h} of SB fabrics. The

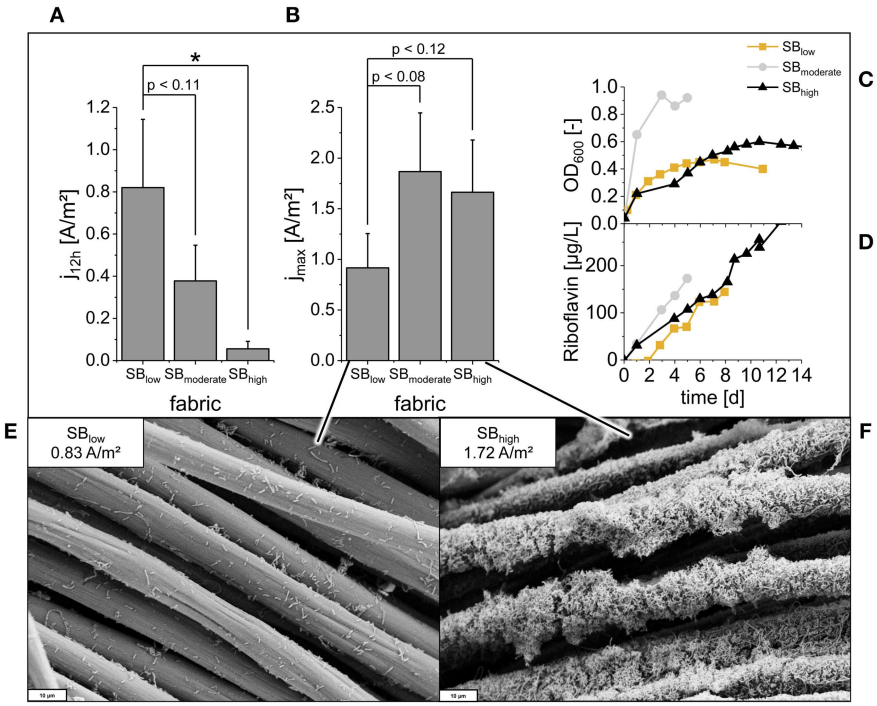

FIGURE 5 | (A) Maximum current densities j_{max}, **(B)** startup current density j_{12h} (both normalized to 2D projected surface area), **(C)** examples for planktonic growth, and **(D)** riboflavin production achieved with fabric electrodes made from stretch-broken yarn (SB) with increasing carbon contents (low, moderate, high). **(A,B)** Are average values and standard deviations from triplicates **(C,D)**, are representative single experiments. Asterisks mark significance levels of $p < 0.05$ (two-sampled *t*-test), other *p*-values lower than 0.12 are also given. **(E,F)**: SEM images of example fabrics SB_{low}/SB_{high}, which were taken after 15 days from reactors sharing identical inocula; scale bars = 10 µm. Current density values displayed in images **(E,F)** correspond to the sampling time point (end of experiment).

same overview is given for CM fabrics in **Figure 6**. Example full electrochemical datasets for both fabric types are given in **Figures S6**, **S7**, respectively.

In the case of stretch-broken fabrics, a substantial increase in maximum current density j_{max} (by average of 100%) and $OD_{600-max}$ (by average of 60%) was linked to an increased filament conductivity from SB_{low} to $SB_{moderate}$ (**Figure 5B**). With the second graphitization step from $SB_{moderate}$ to SB_{high}, j_{max} stayed at similar levels as $SB_{moderate}$ and the $OD_{600-max}$ even fell back to levels of SB_{low} (**Figure 5C**). In total, the increased carbon content from SB_{low} to SB_{high} came along with a progressive limitation on initial current generation (reduction of j_{12h} by ∼50 and 90% for $SB_{moderate}$ and SB_{high}, respectively, **Figure 5A**). This clear trend was not correlated with planktonic growth, which was similar for SB_{low} and SB_{high}, but much enhanced—both regarding growth rate and $OD_{600-max}$ – for $SB_{moderate}$ (**Figure 5C**). The production of the electron mediator riboflavin was similar in SB of all carbon contents, and only slightly enhanced in $SB_{moderate}$ (**Figure 5D**).

Two electrode samples, which were taken from reactors sharing identical inoculum and identical starting time points, were selected for SEM imaging. The carbonized SB_{low} (**Figure 5E**) displayed the typical thin biofilm (isolated single cells) of *S. oneidensis* on carbon based electrodes under anaerobic conditions, which has been observed in our lab and elsewhere (Rosenbaum et al., 2010). In contrast, the final biomass was exceptionally dense on the highly graphitized SB_{high} fabric (**Figure 5F**), displaying multiple cell layers. The cells were tightly packed in the biofilm and by this, formed continuous connections between individual filaments. Intruding oxygen can be responsible for an increased biomass on the electrode as well as planktonic growth and flavin production (TerAvest et al., 2014). However, the CE for the respective SB_{high} reactor was 44%, which is higher than results from other studies that claim close to anaerobic conditions (Rosenbaum et al., 2011; Engel et al., 2019), and it was also very close to the average CE of the plate reactor setup. We consequently consider the extraordinary biofilm on SB_{high} to be truly related to the electrode properties.

In CM fabrics, increased filament conductivity is not boosting j_{max}, and even has an adverse effect in the case of $CM_{moderate}$ fabrics (**Figure 6B**). The latter was in accordance with a slightly reduced number of cells on $CM_{moderate}$ compared to CM_{low} samples (**Figures 6E,F**). In this case, the handling of the graphitized fabric might have introduced some unintended breaks in the brittle filaments, which increased the fabric resistivity. In general, a reduced startup current production with increasing carbon content was observed, the decrease being especially strong between CM_{low} and the first graphitization step $CM_{moderate}$ (**Figure 6A**, reduction of j_{12h} by ∼85 and 93% for $CM_{moderate}$ and CM_{high}, respectively). This is also

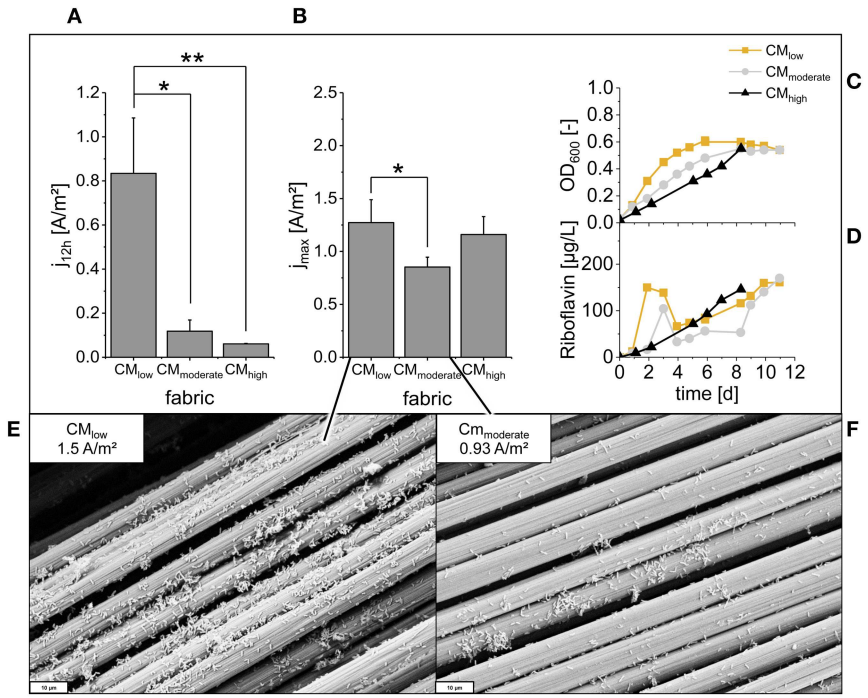

FIGURE 6 | (A) Startup current density j_{12h} **(B)**, maximum current densities j_{max} (both normalized to 2D projected surface area) **(C)**, planktonic growth, and **(D)** riboflavin production achieved with fabric electrodes made from continuous multifilament (CM) with increasing carbon contents (low, moderate, high). **(A,B)** Are average values and standard deviations from triplicates (duplicates for CM_{high}), **(C,D)** are representative single experiments. Single/double asterisks mark significance levels of $p < 0.05$ and $p < 0.01$ (two-sampled *t*-test). **(E,F)**: SEM images of the of CM_{low}/$CM_{moderate}$ electrodes, which were taken after 13 days from reactors sharing identical inocula; scale bars = 10 µm. Current density values displayed in images **(E,F)** correspond to the sampling time point (end of experiment).

correlated to a faster initial planktonic growth in the CM_{low} reactor compared to the other two reactors, while the final OD_{600} was not affected and reached similar values in all CM levels (**Figure 6C**). The fast current generation of CM_{low} was also accompanied by a fast initial increase in riboflavin concentration. After j_{max} was reached with CM_{low}, riboflavin levels dropped sharply in all 3 replicates, to continue with a slower increase after the drop (**Figure 6D**). $CM_{moderate}$ showed a similar trend of increase-drop-increase of riboflavin levels, but less pronounced. In CM_{high}, the riboflavin levels increased continuously corresponding to the OD_{600} increase.

DISCUSSION

CF based textile fabrics are a popular electrode material for BES, primarily because they offer a large surface area for bacteria-electrode interactions. However, the growing CF market and new applications have created a broad spectrum of many more tunable material characteristics. Growing production capacities result in dropping prices, which may soon allow for economic electrode designs for BES (Morgan, 2005; Das et al., 2016). In order to assess the specific effect of characteristics like the specific electrical resistance of a CF type on the final electrode performance in BES, suitable single fiber and fabric samples were selected and/or modified to enable a systematic investigation.

Pure cultures of the electroactive model organism *S. oneidensis* MR-1 were used for the performance screening of CF electrodes. The multiple, consecutive experiments performed in this work require a reliable inoculum performance over a certain period of time. While electroactive mixed cultures require an advanced level of practical experience in order to maintain a stable inoculum, the use of pure cultures provides a straightforward approach. *S. oneidensis* was chosen over other electroactive bacteria like e.g., *G. sulfurreducens* for its comparatively fast growth, easy handling and robust anodic electroactivity even in the presence of oxygen leaking into the system; all of which reduced the complexity and time-consumption of the experimental setups presented here. The inherent low current densities of *S. oneidensis* (Kipf et al., 2014) do not affect the main purpose of the tests to compare electrode materials against each other.

Desizing Is an Important Step in the Production of Carbon Fiber Based Electrodes

While SB fabrics get their sizing removed before the last production step, CM fabrics are always coated by a sizing (**Figure 1**). Our investigations highlight the importance of proper desizing for standard and cheap commercial CM fabrics. The impact of the electrically insulating sizing on the electrode

performance is especially great for large and voluminous carbon fiber based electrodes. Here, the desizing method has to be adapted (e.g., by prolonging process times) and complete removal of the sizing has to be ensured via e.g., TGA, as demonstrated here. Our results are supported by the work of other authors, who mentioned necessary "pretreatment" methods in order to turn "carbon mesh" (presumably a CM fabric) into electrochemically active anodes for power production in MFCs (Wang et al., 2009). The authors used TGA to follow the effect of their pretreatment and recorded a weight loss. The described thermal and solvent-based (acetone) cleaning procedures represent common industrial desizing methods and were all able to drastically increase the MFC performance over MFCs with an untreated "carbon mesh" on short term operation (17 days). The other material, which is referred to as "carbon cloth," did not have to be "pretreated" (presumably a PANOX SB fabric, but unfortunately no material specifications were provided).

Among the presented options, we recommend the use of thermal desizing as a waste-free method. Furthermore, the gaseous process medium leaves a clean fabric surface without the need for extensive washing steps. The thermal desizing can easily be scaled and implemented into existing process chains (technically, it is not much different from the equipment for carbonization). In a broader context, the thermal method could be used for a combined desizing and chemical surface activation by simply adapting the process gas. This can be O_2 or ambient air, or as shown by Wang et al. (2009), also ammonia modifies the carbon surface. In these cases, however, a strict process control is mandatory in order to only modify the filament surface and maintain good mechanical and electrical properties of the carbon fibers.

Chemical Modification of the Carbon Surface May Enhance Electrode Performance in Certain Cases

According to our results, the effect of surface activation cannot be generalized and depends on the fiber. This is not surprising in the light of the great spectrum of commercial products and their material properties. Although identical treatments were applied to the almost equivalent fibers HTS40 and CT50, the effects were only marginal in HTS40, but strong in CT50 CF. In this case, the increase of j_{12h} for pre-treated fibers could be correlated with an increase in hydrophilicity. The same effects on fiber surface and j_{12h} were achieved by increasing the C-content (**Figures 5A**, **6A**). Furthermore, slightly elevated arithmetic means of j_{12h} of air plasma and electrolytically activated HTS40 CF compared to others were observed, which fit to high amounts of both N and O containing functional residues introduced by these treatments. A higher diversity of functional residues probably offers more options for bacterial cells and biochemical molecules to interact with the filament surfaces in the beginning of the experiment.

The relationship between enhanced BES startup and a hydrophilic electrode surface has also been observed by Guo et al. (2013), who attributed a faster startup of mixed culture bioanodes to increased surface hydrophilicity of activated glassy carbon. In their case, the final current densities were also altered and high currents have been related to an increased selectivity of the activated surfaces for electroactive microorganisms. In other studies, hydrophilicity and positive charged N and O containing functional groups always enhanced the startup of the BES (and hydrophobic surfaces prolonged startup) (Flexer et al., 2013; Guo et al., 2013, 2014; Li et al., 2014; Liu et al., 2014; Santoro et al., 2014; Cornejo et al., 2015), but only in few cases, a long-term enhancement on j_{max} was observed, and if so, only for mixed culture derived systems (Guo et al., 2013, 2014; Liu et al., 2014). In this work, a pure culture of electroactive microorganisms was used. Hence, the lack of competitiveness between microorganisms might be the reason for lacking effect of surface activation on j_{max}. Consequently, the additional surface activation is not expected to improve the overall performance of pure culture BES. The only benefit is the faster startup of freshly inoculated electrodes, which is mainly relevant for batch operation.

Finally, a closer look reveals that j_{12h} of the CT50 was promoted to the level of an untreated HTS40 after surface activation (**Figures 3A,B**). We postulated that the cause for the difference has to originate in the production process parameters, which certainly differ between manufacturers. These may generate e.g., activated surfaces (prior to sizing, **Figure 1**) that even stay chemically stable during the desizing treatment applied for our BES experiments. We conclude that a thorough selection of commercial fibers and close communication with the manufacturers may possibly replace the second surface activation that we intended to add to the general production chain of carbon fibers.

Synergistic Effect of High Filament Conductivity and Free Filament Ends Boosts Bacterial Current Generation

In a perfect graphite crystal, the electrical conductivity along the planes is 10^4 fold higher than perpendicular to the planes (Dutta, 1953). In CF, the anisotropy is weaker, since the graphitic planes are only close to parallel and below 100 C at.%. However, the electrical conductivity may still exceed one order of magnitude in-filament direction compared to through-filament direction (Windhorst and Blount, 1997). The discrepancy is higher in graphitized fibers, which are closer to a perfect graphitic structure. In the most common type of carbon fibers, the multifilament roving (CM), only the longitudinal filament surface is available for bacterial interaction, whereas stretch-broken yarns (SB) allow for a better accessibility of the filament conductivity at the cross sections. We have demonstrated that these free filament ends are able to enhance bacterial current generation when introduced into CM single fiber electrodes (configuration Tx/Dx, chapter Effect of Fiber Type on Bacterial Current Generation).

Moving from single fiber to fabric level, we could further elaborate on the role of free filament ends in SB (chapter Effect of Filament Conductivity and Fiber Type on Bacterial Current Generation). With this yarn type, an increased filament conductivity was responded by an enhanced bacterial current generation (**Figure 5B**). In CM fabrics, which lack free filament

ends, such an effect was consequently not observed (**Figure 6B**). Likewise to our findings in SB fabrics, Baudler et al. (2015) have shown that the current generation of electroactive biofilms can be enhanced by using highly conductive materials like silver and copper instead of carbon (given that electrode potentials are low enough to prevent corrosion). Hence, the electron discharge to the electrode surface does represent a bottle neck in bacterial current generation despite their low turnover rates compared to e.g., metal electrocatalysts. It is still remarkable, though, to which high extent (∼+ 100%) the negligible surface area of free filament ends influenced the overall electrode performance compared to the current increase of about 40% for switching from a graphite to a copper electrode reported by Baudler et al. (2015). The µm-scale roughness of SB is not considered to be responsible for the high current generation, since the scale is not substantially different from the biofilm thickness (Moß et al., 2019). The beneficial effects of (1) free filament ends, and (2) elevated filament conductivity are probably synergistic, making graphitized SB fabrics an excellent electron sink, which triggers an efficient extracellular electron transfer.

This consideration is supported by a fast initial planktonic growth compared to a slower current increase in the moderately graphitized fabric $SB_{moderate}$ (**Figure S6**). It is known that both planktonic cells and biofilms of *S. oneidensis* MR-1 rely on soluble electron mediators for their extracellular electron transfer (Marsili et al., 2008). The soluble riboflavin in $SB_{moderate}$ was only slightly enhanced over SB_{low}, but the concentration in the biofilm was possibly very high. Furthermore, the high amount of planktonic cells (**Figure 5C**) that can discharge electrons to these flavins might already explain high j_{max} in $SB_{moderate}$. When $SB_{moderate}$ was further graphitized to SB_{high}, the role of the planktonic biomass decreased but instead, a multilayer biofilm was observed (**Figure 5F**). The link between high current densities and thick biofilms has been also observed in mixed culture biofilms (Santoro et al., 2014; Baudler et al., 2015), but it is unusual for anaerobically grown *S. oneidensis* (Rosenbaum et al., 2010). With the electrode being the main electron acceptor in this system, the thick biofilm on SB_{high} could only be sustained by an efficient interaction of the bacteria with the electrode. Since we have not analyzed the direct electron transfer via membrane-bound c-type cytochromes, the exact mechanism remains unclear. A high mediator concentration in the biofilm with probably enhanced electron discharge toward the electrode surface might serve as explanation. The presence of long cell bodies (visible in the bottom right section of **Figure 5F**) is also a hint that *S. oneidensis* cells formed efficient links between each other to fully exploit the free filament ends. Furthermore, the membrane-nanowires of *S. oneidensis* can exceed several cell lengths and might have added up to the inter-cell connections (Pirbadian et al., 2014).

Despite the high j_{max} of graphitized SB fabrics, the adverse effect of elevated C-content on startup current j_{12h} cannot be neglected. Since the effect was independent of the fiber type, it can be related to the increased purity of the CF surface, i.e., its increased hydrophobicity (**Figures 5A**, **6A**). This even seemed to affect j_{max} as observed in the graphitized $CM_{moderate}$ fabrics (**Figure 6B**). In SB fabrics, hydrophobicity probably counteracted increased filament conductivity, and consequently a higher graphitization (SB_{high}) than the commercial level ($SB_{moderate}$) did not further push j_{max}. One might argue that the prolonged startup time will not be critical for the actual applications or only relevant for batch operations, since the final OD_{600} was not significantly affected (**Figure 5C**). However, there are more indications in literature that a hydrophobic electrode surface could reduce final current densities due to reduced selectivity for electroactive microorganisms from mixed culture inocula (Guo et al., 2013). A surface activation of graphitized SB fabrics might be a technical solution, since it can reduce the startup time (chapter Characterization of Surface Activated CF in Single Fiber BES), but the additional process steps would clearly add up to the electrode cost. In summary, we propose (moderately) graphitized SB fabrics as a viable electrode material mainly for pure culture BES, especially when continuously operated. The configuration in a woven fabric allows for further engineering of highly porous, yet mechanically stable electrodes, which are useful for good mass transfer in stirred reactors. For large-scale mixed culture BES applications, however, CM fabrics might be a more economic choice. But also for CM, we show that the configuration of the fabric determines whether the full potential of the fibers can be exploited. The best configuration in the single fiber BES was the open configuration D0/T0 (**Figure 4**), which allows for an optimized accessibility of single filaments, but is impractical for most applications. Fabrics that come closest to conserve this configuration are thin unidirectional non-wovens or woven fabrics of low yarn input.

SUMMARY AND OUTLOOK

Carbon fiber woven fabrics are a versatile electrode material that can be customized with a high reproducibility. Their excellent trade-off between good mechanical stability, flexibility, electrical conductivity, and material exploitation makes them suitable materials for the wide variety of novel BES applications. This study shows that the potential of carbon fiber fabrics can be comprehensively exploited and there are several factors to be customized for the specific BES application. In the light of the diversity of CF and thereof derived products, we recommend that BES studies using such electrodes report the specific CF material properties and the applied treatments such as desizing and surface activation. This way, research results may be translated to a comprehensive adaptation of process parameters and push forward the industrial implementation of BES-oriented CF product lines. With the above results, we focused on identifying the relevant fiber material properties and found graphitized, stretch-broken fiber based woven fabrics to be interesting for stirred pure culture BES. For low-tech applications in highly competitive technological fields, such as wastewater treatment, the use of less costly fabrics based on continuous multifilament rovings is recommended. For these fabrics, we point out that a proper removal of the sizing is crucial for efficient bacteria-electrode interaction and should be verified by, e.g., TGA analysis. We also looked into different chemical surface activation methods in order to increase the biocompatibility of

the carbon fiber surface. The most suitable methods are such that introduce both nitrogen and oxygen containing residues and increase the hydrophilicity of the carbon surface. We could not confirm an impact of surface activation on maximum current density, but only on the reduction of startup time. However, the effect depended strongly on the fiber and we found that there are commercial fibers that already come with sufficiently biocompatible surfaces. We concluded that a surface activation is of limited use for pure culture BES lacking microbial competition during startup. Nevertheless, it may be useful for mixed culture BES to enhance selection of highly electroactive biofilm members.

DATA AVAILABILITY

All relevant data are included in this manuscript and the corresponding **Supplementary Material**.

AUTHOR CONTRIBUTIONS

LP coordinated the study, designed, conducted and analyzed all BES experiments, and prepared the manuscript. PH coordinated and performed the fiber and fabric material selection, supervised and analyzed their physical characterization experiments, and co-prepared the manuscript. SS coordinated and supervised the desizing, surface activation experiments and revised the manuscript. VR conducted SEM sample preparation and analyses in chapter Effect of Filament Conductivity and Fiber Type on Bacterial Current Generation and Revised the Manuscript. TG advised on all CF work, discussed results, and revised the manuscript. LB discussed the work and revised the manuscript. MR conceived the work, advised on the experimental plan, discussed experiments, and revised the manuscript.

FUNDING

The IGF research project (IGF Grant No. 19047 N) of the research association Forschungskuratorium Textil e.V., Reinhardtstraße 14-16, 10117 Berlin was funded via the AiF within the program for supporting the industrial Collective Research (IGF) from funds of the Federal Ministry of Economic Affairs and Energy (BMWi). Further funding was provided by the German Federal Ministry of Education and Research (BMBF) under Grant No. 031B0087A.

ACKNOWLEDGMENTS

We are very thankful to Almut Schwenke (SGL Carbon, Germany), who provided CF materials, discussed their properties, provided graphitization services, and revised the manuscript. We are also grateful to Sebastian Wittig (Diener electronic GmbH & Co. KG, Germany) for providing plasma activation services and expertise regarding surface activation. Furthermore, we wish to thank Myong-Hun Jung, Tobias Bolz, and Felicitas Schmitz for their great contribution to the experimental work. We also thank Jürgen Klimke (CARBO-TEX GmbH, Germany), who provided T300 fabrics and was always available for helpful advice.

SUPPLEMENTARY MATERIAL

The Supplementary Material for this article can be found online at: https://www.frontiersin.org/articles/10.3389/fenrg.2019.00100/full#supplementary-material

REFERENCES

Alexander, M. R., and Jones, F. R. (1996). Effect of electrolytic oxidation upon the surface chemistry of type A carbon fibres: III. Chemical state, source and location of surface nitrogen. *Carbon* 34, 1093–1102. doi: 10.1016/0008-6223(96)00061-9

Artyushkova, K., Cornejo, J. A., Ista, L. K., Babanova, S., Santoro, C., and Atanassov, P. (2015). Relationship between surface chemistry, biofilm structure, and electron transfer in *Shewanella* anodes. *Biointerphases* 10:019013. doi: 10.1116/1.4913783

Baudler, A., Schmidt, I., Langner, M., Greiner, A., and Schröder, U. (2015). Does it have to be carbon? Metal anodes in microbial fuel cells and related bioelectrochemical systems. *Energy Environ. Sci.* 8, 2048–2055. doi: 10.1039/C5EE00866B

Beg, Q. K., Zampieri, M., Klitgord, N., Collins, S. B., Altafini, C., Serres, M. H., et al. (2012). Detection of transcriptional triggers in the dynamics of microbial growth: application to the respiratorily versatile bacterium *Shewanella oneidensis*. *Nucleic Acids Res.* 40, 7132–7149. doi: 10.1093/nar/gks467

Blanchet, E., Erable, B., De Solan, M.-L., and Bergel, A. (2016). Two-dimensional carbon cloth and three-dimensional carbon felt perform similarly to form bioanode fed with food waste. *Electrochem. Commun.* 66, 38–41. doi: 10.1016/j.elecom.2016.02.017

Champigneux, P., Renault-Sentenac, C., Bourrier, D., Rossi, C., Delia, M.-L., and Bergel, A. (2018). Effect of surface nano/micro-structuring on the early formation of microbial anodes with *Geobacter sulfurreducens*: experimental and theoretical approaches. *Bioelectrochemistry* 121, 191–200. doi: 10.1016/j.bioelechem.2018.02.005

Chen, S., Hou, H., Harnisch, F., Patil, S. A., Carmona-Martinez, A. A., Agarwal, S., et al. (2011). Electrospun and solution blown three-dimensional carbon fiber non-wovens for application as electrodes in microbial fuel cells. *Energy Environ. Sci.* 4, 1417–1421. doi: 10.1039/c0ee00446d

Cornejo, J. A., Jopez, C., Babanova, S., Santoro, C., Artyushkova, K., Ista, L., et al. (2015). Surface modification for enhanced biofilm formation and electron transport in *Shewanella* anodes. *J. Electrochem. Soc.* 162, H597–H603. doi: 10.1149/2.0271509jes

Das, S., Warren, J., West, D., and Schexnayder, S. M. (2016). *Gobal Carbon Fiber Composites Supply Chain Competitiveness Analysis*. Energy Transportation Science Division, Oak Ridge National Laboratory. doi: 10.2172/1254094

Donovan, C., Dewan, A., Heo, D., Lewandowski, Z., and Beyenal, H. (2013). Sediment microbial fuel cell powering a submersible ultrasonic receiver: new approach to remote monitoring. *J. Power Sources* 233, 79–85. doi: 10.1016/j.jpowsour.2012.12.112

Dutta, A. K. (1953). Electrical conductivity of single crystals of graphite. *Phys. Rev.* 90, 187–192. doi: 10.1103/PhysRev.90.187

Engel, C., Schattenberg, F., Dohnt, K., Schröder, U., Müller, S., and Krull, R. (2019). Long-term behavior of defined mixed cultures of *Geobacter sulfurreducens* and *Shewanella oneidensis* in bioelectrochemical systems. *Front. Bioengineer. Biotechnol.* 7:60. doi: 10.3389/fbioe.2019.00060

Ewing, T., Ha, P. T., and Beyenal, H. (2017). Evaluation of long-term performance of sediment microbial fuel cells and the role of natural

resources. *Appl. Energy* 192, 490–497. doi: 10.1016/j.apenergy.2016.08.177

Flexer, V., Marque, M., Donose, B. C., Virdis, B., and Keller, J. (2013). Plasma treatment of electrodes significantly enhances the development of anodic electrochemically active biofilms. *Electrochim. Acta* 108, 566–574. doi: 10.1016/j.electacta.2013.06.145

Gajda, I., Greenman, J., and Ieropoulos, I. A. (2018). Recent advancements in real-world microbial fuel cell applications. *Curr. Opin. Electrochem.* 11, 78–83. doi: 10.1016/j.coelec.2018.09.006

Guo, K., Freguia, S., Dennis, P. G., Chin, X., Donose, B. C., Keller, J., et al. (2013). Effects of surface charge and hydrophobicity on anodic biofilm formation, community composition, and current generation in bioelectrochemical systems. *Environ. Sci. Technol.* 47, 7563–7570. doi: 10.1021/es400901u

Guo, K., Soeriyadi, A. H., Patil, S. A., Prévoteau, A., Freguia, S., Gooding, J. J., et al. (2014). Surfactant treatment of carbon felt enhances anodic microbial electrocatalysis in bioelectrochemical systems. *Electrochem. Commun.* 39, 1–4. doi: 10.1016/j.elecom.2013.12.001

He, G., Gu, A., He, S., Schröder, U., Chen, S., and Hou, H. (2011). Effect of fiber diameter on the behavior of biofilm and anodic performance of fiber electrodes in microbial fuel cells. *Bioresour. Technol.* 102, 10763–10766. doi: 10.1016/j.biortech.2011.09.006

Hiegemann, H., Herzer, D., Nettmann, E., Lübken, M., Schulte, P., Schmelt, K.-G., et al. (2016). An integrated 45 L pilot microbial fuel cell system at a full-scale wastewater treatment plant. *Bioresour. Technol.* 218, 115–122. doi: 10.1016/j.biortech.2016.06.052

Ieropoulos, I. A., Stinchcombe, A., Gajda, I., Forbes, S., Merino-Jimenez, I., Pasternak, G., et al. (2016). Pee power urinal—microbial fuel cell technology field trials in the context of sanitation. *Environ. Sci.* 2, 336–343. doi: 10.1039/C5EW00270B

Janicek, A., Fan, Y., and Liu, H. (2014). Design of microbial fuel cells for practical application: a review and analysis of scale-up studies. *Biofuels* 5, 79–92. doi: 10.4155/bfs.13.69

Jones, C., and Sammann, E. (1989). *The Effect of Low Power Plasmas on Carbon Fibre Surfaces, ONR-URI Composites Program Technical Report No. 16*. National Center for Composite Material Research at University of Illinois (Champaign, IL). doi: 10.21236/ADA234184

Kipf, E., Koch, J., Geiger, B., Erben, J., Richter, K., Gescher, J., et al. (2013). Systematic screening of carbon-based anode materials for microbial fuel cells with *Shewanella oneidensis* MR-1. *Bioresour. Technol.* 146, 386–392. doi: 10.1016/j.biortech.2013.07.076

Kipf, E., Zengerle, R., Gescher, J., and Kerzenmacher, S. (2014). How does the choice of anode material influence electrical performance? A comparison of two microbial fuel cell model organisms. *ChemElectroChem*. 1, 1849–1853. doi: 10.1002/celc.201402036

Kozlowski, C., and Sherwood, P. M. A. (1986). X-ray photoelectron spectroscopic studies of carbon fibre surfaces vii-electrochemical treatment in ammonium salt electrolytes. *Carbon.* 24, 357–363. doi: 10.1016/0008-6223(86)90238-1

Li, B., Zhou, J., Zhou, X., Wang, X., Li, B., Santoro, C., et al. (2014). Surface modification of microbial fuel cells anodes: approaches to practical design. *Electrochim. Acta* 134, 116–126. doi: 10.1016/j.electacta.2014.04.136

Liu, J., Liu, J., He, W., Qu, Y., Ren, N., and Feng, Y. (2014). Enhanced electricity generation for microbial fuel cell by using electrochemical oxidation to modify carbon cloth anode. *J. Power Sources* 265, 391–396. doi: 10.1016/j.jpowsour.2014.04.005

Lu, M., Chan, S., Babanova, S., and Bretschger, O. (2017a). Effect of oxygen on the per-cell extracellular electron transfer rate of *Shewanella oneidensis* MR-1 explored in bioelectrochemical systems. *Biotechnol. Bioeng.* 114, 96–105. doi: 10.1002/bit.26046

Lu, M., Chen, S., Babanova, S., Phadke, S., Salvacion, M., Mirhosseini, A., et al. (2017b). Long-term performance of a 20-L continuous flow microbial fuel cell for treatment of brewery wastewater. *J. Power Sources* 356, 274–287. doi: 10.1016/j.jpowsour.2017.03.132

Marsili, E., Baron, D. B., Shikhare, I. D., Coursolle, D., Gralnick, J. A., and Bond, D. R. (2008). *Shewanella* secrets flavins that mediate extracellular electron transfer. *PNAS* 105, 3968–3973. doi: 10.1073/pnas.0710525105

Morgan, P. (2005). *Carbon Fibers and Their Composites.* Boca Raton, FL: CRC Press, Taylor and Francis Group. doi: 10.1201/9781420028744

Moß, C., Patil, S. A., and Schröder, U. (2019). Scratching the surface—how decisive are microscopic surface structures on growth and performance of electrochemically active bacteria? *Front. Energy Res.* 7:18. doi: 10.3389/fenrg.2019.00018

Pierra, M., Golozar, M., Zhang, X., Prévoteau, A., Volder, M. D., Reynaerts, D., et al. (2018). Growth and current production of mixed culture anodic biofilms remain unaffected by sub-microscale surface roughness. *Bioelectrochemistry* 122, 213–220. doi: 10.1016/j.bioelechem.2018.04.002

Pinchuk, G. E., Geydebrekht, O. V., Hill, E. A., Reed, J. L., Konopka, A. E., Beliaev, A. S., et al. (2011). Pyruvate and lactate metabolism by *Shewanella oneidensis* MR-1 under fermentation, oxygen limitation, and fumarate respiration conditions. *Appl. Environ. Microbiol.* 77, 8234–8240. doi: 10.1128/AEM.05382-11

Pirbadian, S., Barchinger, S. E., Leung, M. L., Suk Byun, H. K., Jangir, Y., Bouhenni, R. A., et al. (2014). *Shewanella oneidensis* MR-1 nanowires are outer membrane and periplasmic extensions of the extracellular electron transport components. *PNAS* 111, 12883–12888. doi: 10.1073/pnas.1410551111

Qian, H., Bismarck, A., Greenhalgh, E. S., and Shaffer, M. S. P. (2010). Carbon nanotube grafted carbon fibres: a study of wetting and fibre fragmentation. *Compos. Part A Appl. Sci. Manuf.* 41, 1107–1114. doi: 10.1016/j.compositesa.2010.04.004

Raes, S. M. T., Jourdin, L., Buisman, C. J. N., and Strik, D. P. B. T.B. (2016). Continuous long-term bioelectrochemical chain elongation to butyrate. *ChemElectroChem* 4:386. doi: 10.1002/celc.201600587

Rosenbaum, M., Cotta, M. A., and Angenent, L. T. (2010). Aerated *Shewanella oneidensis* in continuously fed bioelectrochemical systems for power and hydrogen production. *Biotechnol. Bioeng.* 105, 880–888. doi: 10.1002/bit.22621

Rosenbaum, M. A., Bar, H. Y., Beg, Q. K., Segrè, D., Booth, J., Cotta, M. A., et al. (2011). *Shewanella oneidensis* in a lactate-fed pure-culture and a glucose-fed co-culture with *Lactococcus lactis* with an electrode as electron acceptor. *Bioresour. Technol.* 102, 2623–2628. doi: 10.1016/j.biortech.2010.10.033

Santoro, C., Arbizzani, C., Erable, B., and Ieropoulos, I. (2017). Microbial fuel cells: from fundamentals to applications. A review. *J. Power Sour.* 356, 225–244. doi: 10.1016/j.jpowsour.2017.03.109

Santoro, C., Guilizzoni, M., Correa Baena, J. P., Pasaogullari, U., Casalegno, A., Li, B., et al. (2014). The effects of carbon electrode surface properties on bacteria attachment and start up time of microbial fuel cells. *Carbon.* 67, 128–139. doi: 10.1016/j.carbon.2013.09.071

Severini, F., Formaro, L., Pegoraro, M., and Posca, L. (2002). Chemical modification of carbon fiber surfaces. *Carbon.* 40, 735–741. doi: 10.1016/S0008-6223(01)00180-4

Streeck, J., Hank, C., Neuner, M., Gil-Carrera, L., Kokko, M., Pauliuk, S., et al. (2018). Bio-electrochemical conversion of industrial wastewater combined with downstream methanol synthesis—an economic- and life cycle assessment. *Green Chem.* 20, 2742–2762. doi: 10.1039/C8GC00543E

Tender, L. M., Gray, S. A., Groveman, E., Lowy, D. A., Kauffman, P., Melhado, J., et al. (2008). The first demonstration of a microbial fuel cell as a viable power supply: powering a meteorological buoy. *J. Power Sources* 179, 571–575. doi: 10.1016/j.jpowsour.2007.12.123

TerAvest, M. A., Rosenbaum, M. A., Kotloski, N. J., Gralnick, J. A., and Angenent, L. T. (2014). Oxygen allows *Shewanella oneidensis* MR-1 to overcome mediator washout in a continuously fed bioelectrochemical system. *Biotechnol. Bioeng.* 111, 692–699. doi: 10.1002/bit.25128

Walter, X. A., Merino-Jiménez, I., Greenman, J., and Ieropoulos, I. (2018). PEE POWER® urinal II—Urinal scale-up with microbial fuel cell scale-down for improved lighting. *J. Power Sources* 392, 150–158. doi: 10.1016/j.jpowsour.2018.02.047

Wang, X., Cheng, S., Feng, Y., Merrill, M. D., Saito, T., and Logan, B. E. (2009). Use of carbon mesh anodes and the effect of different pretreatment methods on power production in microbial fuel cells. *Environ. Sci. Technol.* 43, 6870–6874. doi: 10.1021/es900997w

Wang, Y., Zhao, Y., Xu, L., Wang, W., Doherty, L., Tang, C., et al. (2017). Constructed wetland integrated microbial fuel cell system: looking back, moving forward. *Water Sci. Technol.* 76, 471–477. doi: 10.2166/wst.2017.190

Watson, V. J., and Logan, B. E. (2009). Power production in MFCs inoculated with *Shewanella oneidensis* MR-1 or mixed cultures. *Biotechnol. Bioeng.* 105, 489–498. doi: 10.1002/bit.22556

Windhorst, T., and Blount, G. (1997). Carbon-carbon composites: a summary of recent developments and applications. *Mater. Design* 18, 11–15. doi: 10.1016/S0261-3069(97)00024-1

Conflict of Interest Statement: The authors declare that the research was conducted in the absence of any commercial or financial relationships that could be construed as a potential conflict of interest.